Cell Cycle 12:16, 2636–2642; August 15, 2013; © 2013 Landes Bioscience

Antiapoptotic activity of argon and xenon

Sabrina Spaggiari[1,2,3], Oliver Kepp[1,2,3], Santiago Rello-Varona[1,2,3], Kariman Chaba[1,2,3], Sandy Adjemian[1,2,3], Jan Pype[4], Lorenzo Galluzzi[1,5,6], Marc Lemaire[4], and Guido Kroemer[3,5,6,7,8,*]

[1]INSERM; U848; Villejuif, France; [2]Institut Gustave Roussy; Villejuif, France; [3]Université Paris Sud/Paris XI; Le Kremlin Bicêtre, France; [4]Air Liquid R&D Medical Gases Group, Air Liquide-Claude Delorme Research Center; Jouy-en Josas, France; [5]Université Paris Descartes/Paris V; Sorbonne Paris Cité; Paris, France; [6]Equipe 11 labellisée par la Ligue Nationale contre le Cancer; Centre de Recherche des Cordeliers; Paris, France; [7]Metabolomics and Cell Biology Platforms; Institut Gustave Roussy; Villejuif, France; [8]Pôle de Biologie; Hôpital Européen Georges Pompidou; AP-HP; Paris, France

Keywords: antimycin A, menadione, mitochondrial membrane permeabilization, rotenone, U2OS cells, Z-VAD-fmk

Abbreviations: $\Delta\psi_m$, mitochondrial transmembrane potential; $DiOC_6(3)$, 3,3′-dihexiloxalo-carbocyanine iodide; DsRed, *Discosoma striata* red fluorescent protein; ER, endoplasmic reticulum; GFP, green fluorescent protein; LD, lethal dose; $mitoK_{ATP}$, mitochondrial ATP-sensitive K; MMP, mitochondrial membrane permeabilization; MTX, mitoxantrone; NMDA, *N*-methyl-*D*-aspartate; PI, propidium iodide; ROI, region of interest; STS, staurosporine

Although chemically non-reactive, inert noble gases may influence multiple physiological and pathological processes via hitherto uncharacterized physical effects. Here we report a cell-based detection system for assessing the effects of pre-defined gas mixtures on the induction of apoptotic cell death. In this setting, the conventional atmosphere for cell culture was substituted with gas combinations, including the same amount of oxygen (20%) and carbon dioxide (5%) but 75% helium, neon, argon, krypton, or xenon instead of nitrogen. The replacement of nitrogen with noble gases per se had no effects on the viability of cultured human osteosarcoma cells in vitro. Conversely, argon and xenon (but not helium, neon, and krypton) significantly limited cell loss induced by the broad-spectrum tyrosine kinase inhibitor staurosporine, the DNA-damaging agent mitoxantrone and several mitochondrial toxins. Such cytoprotective effects were coupled to the maintenance of mitochondrial integrity, as demonstrated by means of a mitochondrial transmembrane potential-sensitive dye and by assessing the release of cytochrome c into the cytosol. In line with this notion, argon and xenon inhibited the apoptotic activation of caspase-3, as determined by immunofluorescence microscopy coupled to automated image analysis. The antiapoptotic activity of argon and xenon may explain their clinically relevant cytoprotective effects.

Introduction

The inhibition or delay of ischemic cell death is an important therapeutic goal, since it widens the temporal window that allows for the (at least partial) recovery of tissues at reperfusion. The signal transduction cascades that mediate cell death upon ischemia/reperfusion have been extensively investigated, yet nowadays limited therapeutic options are available for patients undergoing a cerebral or cardiac ischemic episode. The development of novel interventions that may prevent or retard cell death in this setting, therefore, has major implications for the management of common ischemic disorders of the brain and heart.[1,2]

According to an increasing amount of studies, some noble gases might exert cytoprotective effects that could be harnessed for several clinical applications, including the prevention/inhibition of ischemia/reperfusion-induced tissue damage.[3-5] Noble gases (i.e., helium, argon, krypton, neon, xenon, and radon) are naturally found in a monatomic form. According to the Rutherford-Bohr model, this originates from the fact that the outermost electron shell (also known as valence shell) of these elements is saturated with electrons. Such a unique physicochemical property is visually represented by the position occupied by noble gases in Mendeleev's periodic table and de facto prevents them from forming covalent bonds with other molecules. Thus, noble gases are chemically inert under standard temperature and pressure conditions. Nonetheless, at least some of these elements can interact in a stabilizing fashion with the active site of specific enzymes and receptors.[6,7] Of note, argon and xenon (but less so helium, krypton, neon, and radon) have been shown to mediate consistent neuroprotective,[8-15] cardioprotective,[16-18] and nephroprotective[4,19,20] effects in vitro, ex vivo, and in vivo. Though the molecular mechanisms underlying these observations remain largely undefined, it has been proposed that the cytoprotective effects of noble gases might result from the opening of the mitochondrial ATP-sensitive K

*Correspondence to: Guido Kroemer; Email: kroemer@orange.fr
Submitted: 06/28/2013; Accepted: 07/07/2013
http://dx.doi.org/10.4161/cc.25650

($mitoK_{ATP}$) channels.[16,21] Thus, some inert gases may mediate organoprotective effects via a signaling pathway that overlaps—at least in part—with that activated by ischemic preconditioning.[22]

Cell death can be classified according to the morphological appearance of the lethal process[23,24] or to specific biochemical/functional markers.[25-27] The most common form of regulated cell death, apoptosis, generally manifests with the progressive shrinkage of the cytoplasmic and nuclear compartments followed by blebbing, a peculiar phenomenon that generates discrete apoptotic corpses containing nuclear fragments and relatively intact cytoplasmic organelles.[23,24] Such a morphologically stereotyped form of cell death can be initiated by both extracellular and intracellular cues, which are converted into a lethal response via two distinct, yet partially overlapping, signal transduction cascades.[25,26] In particular, intrinsic apoptosis is activated by a wide variety of intracellular stress conditions (e.g., DNA damage, endoplasmic reticulum stress, Ca^{2+} overload, oxidative stress) and is mediated by a cascade of biochemical events that culminate in widespread mitochondrial membrane permeabilization (MMP).[23,24] Upon MMP, not only is mitochondrial ATP synthesis abrogated as a result of the dissipation of the mitochondrial transmembrane potential ($\Delta\psi_m$), but also, several cytotoxic proteins that normally reside within the mitochondrial intermembrane space, such as cytochrome *c* and apoptosis-inducing factor,[28,29] are released into the cytosol. Extra-mitochondrial cytochrome *c* orchestrates the assembly of the so-called "apoptosome", a supramolecular complex that catalyzes the proteolytic maturation of the central execution of apoptotic cell death, i.e., caspase-3.[25,26]

Here, we report that 2 noble gases, argon and xenon, are able to limit intrinsic apoptosis as stimulated by the broad-spectrum kinase inhibitor staurosporine (STS), the DNA-damaging agent mitoxantrone (MTX), and several mitochondrial toxins. Argon and xenon inhibited several manifestations of STS-induced apoptosis, including $\Delta\psi_m$ dissipation and caspase-3 activation, thus far resembling the widely employed pan-caspase blocker Z-VAD-fmk.

Results and Discussion

Automated fluorescence microscopy reveals the cytoprotective activity of argon and xenon

To evaluate the possible cytoprotective effects of inert gases, we designed an experimental system that allows for the automated fluorescence microscopy-based assessment of cell number upon the culture of human osteosarcoma U2OS cells stably expressing a histone 2B-red fluorescent protein (RFP-H2B) chimera (which labels chromatin) in the presence of pre-determined gas mixtures. Thus, U2OS cells were grown in the presence of a control atmosphere (75% N_2, 20% O_2, and 5% CO_2) or atmospheres in which N_2 was selectively replaced by 6 alternative gases (He, Ne, Ar, Kr, Xe, or N_2O), while O_2 and CO_2 concentrations were kept unaltered (**Fig. 1**). Of note, to avoid possible bias resulting from the gaseous component of culture media, these were invariably pre-saturated with the atmosphere of choice.

Along with the substitution of atmospheric conditions, U2OS cells were placed in drug-free culture medium or in medium supplemented with STS (a broad-spectrum kinase inhibitor that interrupts most—if not all—trophic signaling cascades),[30] mitoxantrone (a DNA-damaging anthracycline),[31] rotenone (an inhibitor of the complex I of the mitochondrial respiratory chain),[32] antimycin A (an inhibitor of the complex III of the mitochondrial respiratory chain),[33] or menadione (a redox-cycling agent that stimulates the overproduction of reactive oxygen species),[34] for 6 or 16 h. At the end of the experiment, culture plates were fixed and processed by a robotized fluorescence microscopy-based imaging platform for the automated quantification of residual cell number.

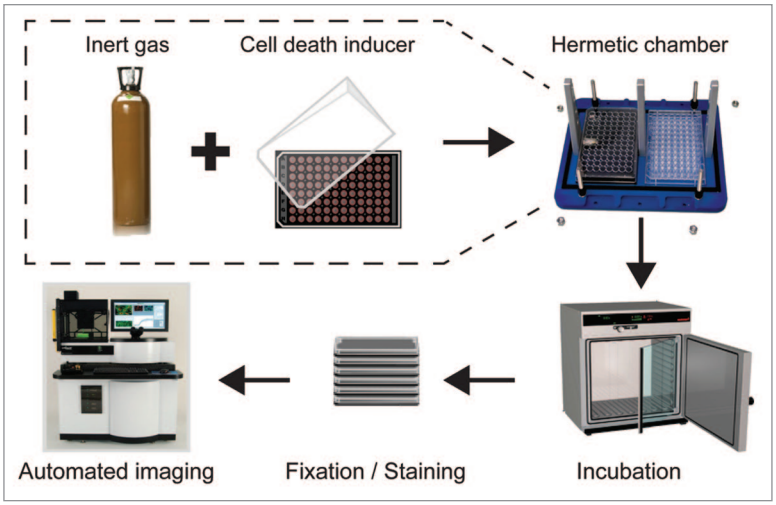

Figure 1. Experimental setup employed in this study. Human osteosarcoma U2OS cells stably expressing a histone 2B-red fluorescent protein (H2B-RFP) chimera were maintained in control conditions or exposed to a panel of cytotoxic compounds within gas tight chambers containing a standard atmosphere (20% O_2, 5% CO_2, and 75% N_2) or a gas mixture in which N_2 was specifically replaced with He, Ne, Ar, Kr, Xe, or N_2O, while O_2 and CO_2 concentrations were kept unaltered. After 6 or 16 h, cells were fixed in the presence of Hoechst 33342, optionally stained for the detection of cytochome *c* release and caspase-3 activation, and subjected to robotized (immuno)fluorescence microscopy followed by automated image acquisition.

This experimental approach revealed that Ar and Xe, but not He, Ne, Kr, and N_2O, can prevent the apparent cell loss (reflecting either antiproliferative effects, either lethal effects, or a combination of both) induced by several distinct cytotoxic agents (**Fig. 2**). The cytoprotective activity of Ar and Xe was nearly complete at an early time point (6 h post-stimulation, **Fig. 2A and C**), yet progressively declined (as demonstrated at 16 h post-stimulation, **Fig. 2B and C**). However, even after a cell death induction period of 16 h, Ar and Xe were able to significantly blunt the cell loss induced by STS and antimycin A (**Fig. 2B and C**).

Collectively, these results suggest that Ar and Xe can counteract the antiproliferative and cytotoxic effects of several agents through a cell-autonomous effect that is measurable in vitro on cultured human cells.

Mechanisms of cytoprotection by argon and xenon

STS is well known to stimulate the intrinsic pathway of apoptosis, which involves an obligatory step of MMP near-to-invariably accompanied by caspase activation.[35,36] Accordingly, human osteosarcoma U2OS cells exposed to STS manifested $\Delta\psi_m$ dissipation, as quantified with the $\Delta\psi_m$-sensitive fluorochrome $DiOC_6(3)$, followed by the loss of plasma membrane integrity, as assessed with the vital dye propidium iodide (PI). The substitution of N_2 with Ar or Xe reduced both such signs of apoptotic cell death, similar to the administration of the pan-caspase inhibitor Z-VAD-fmk (**Fig. 3A and B**). Of note, the administration of Z-VAD-fmk to U2OS cells exposed to STS in the presence of Ar or Xe (rather than of N_2) failed to generate additive cytoprotective effects (**Fig. 3B**), suggesting that Ar and Xe inhibit cell death by acting on a signal transduction pathway that is sensitive to Z-VAD-fmk (and hence presumably involves caspases).

To further substantiate the capacity of Ar and Xe to interfere with the intrinsic pathway of apoptosis, we measured the capacity of these noble gases to limit the cytosolic redistribution of cytochrome *c* and the subsequent activation of caspase-3 as triggered by STS. To this aim, we employed a 2-color fluorescence staining protocol that allows for the combined assessment of cytochrome *c* subcellular localization (changing from a punctuate, filamentous mitochondrial pattern to a diffuse, uniform distribution in the course of apoptosis) and caspase-3 proteolytic activation (generating a neo-epitope which can be recognized by means of specific monoclonal antibodies). Ar and Xe were indeed able to reduce the frequency of cells that, in response to STS, exhibited the mitochondrial release of cytochrome *c* and the activation of caspase-3 (**Fig. 4**).

Taken together, our findings indicate that Ar and Xe effectively inhibit an early step in the cascade of events leading to mitochondrial apoptosis, de facto preventing MMP, cytochrome *c* release, caspase activation, and, hence, avoiding cell death.

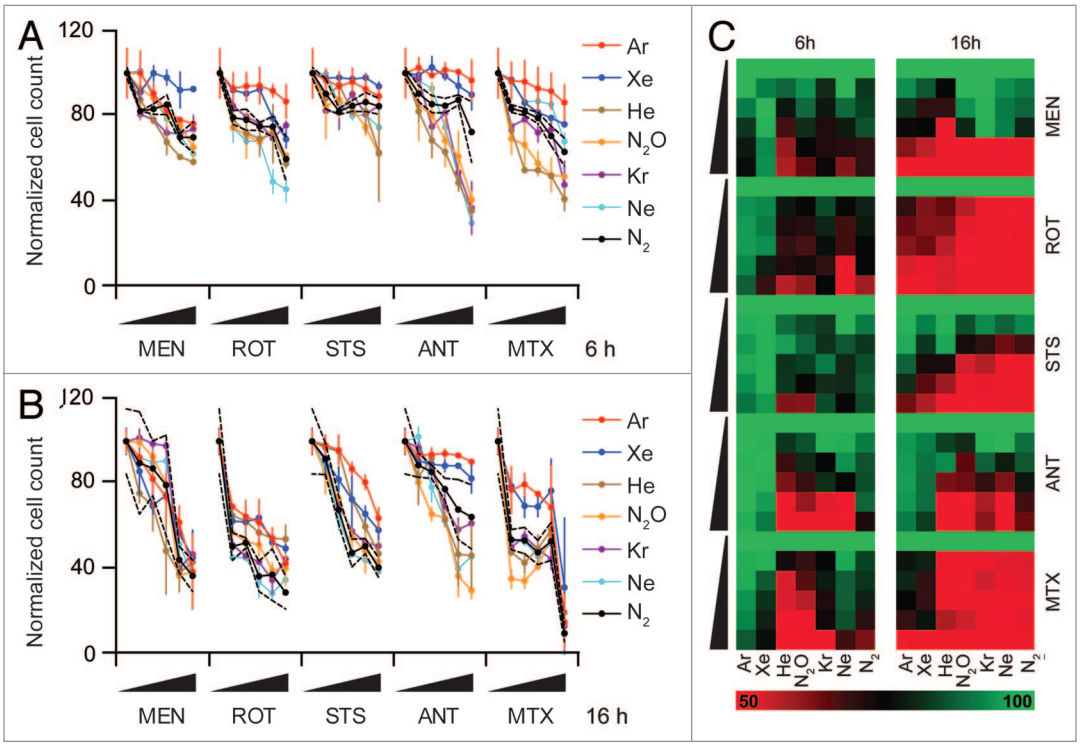

Figure 2. Cytoprotective profile of inert gases. (**A–C**) Human osteosarcoma U2OS cells engineered for the stable expression of a histone 2B-red fluorescent protein (H2B-RFP) chimera were left untreated of exposed to increasing concentrations (0.1×, 0.33×, 1×, 3×, or 10× LD_{50}) of menadione (MEN), rotenone (ROT), staurosporine (STS), antymicin A (ANT), or mitoxantrone (MTX), in control atmospheric conditions (N_2) or in the presence of gasmixtures in which N_2 was specifically replaced with He, Ne, Ar, Kr, Xe, or N_2O for 6 (**A and C**) or 16 h (**B and C**). Thereafter residual cell number was quantified by robotized fluorescence microscopy coupled to automated image analysis. In (**A and B**), quantitative results upon normalization are reported as means ± SD, the upper and lower limits of statistical significance relative to control conditions (standard N_2-containing atmosphere) being indicated by dashed black lines. In (**C**), normalized quantitative data (means) are reported in the form of heat map (dynamic range = 50–100%).

Concluding remarks

The data contained in this report indicate that gas mixtures containing 5% CO_2, 20% O_2, and 75% argon or xenon (as opposed to nitrogen) confer some degree of cytoprotection to cultured human cells. Indeed, the antiproliferative and pro-apoptotic effects of several cytotoxic chemicals, including STS, mitoxantrone, and various mitochondrial poisons, were significantly reduced by the presence of argon or xenon, but not by that of other noble gases, including helium, neon and krypton. In sharp contrast, argon and xenon failed to influence the autophagic response of cultured cells to stress (measured as the aggregation of a fluorescent LC3 variant in cytoplasmic dots upon the administration of rapamycin)[37,38] and the incidence of aberrant mitosis (quantified by means of a fluorescent centrin-based biosensor)[39] (data not shown). Rather, argon and xenon suppressed multiple manifestations of the intrinsic pathway of apoptosis, including two distinct signs of MMP as well as the activation of caspase-3.

Xenon has been shown to mediate prominent neuroprotective,[8,11-15] cardioprotective[16-18] and nephroprotective[4,19,20] effects in vivo. Thus, xenon protects the fetal brain in rat and piglet models of intrauterine perinatal asphyxia, a process that is accompanied by a significant reduction in neuronal apoptosis,[11,12,14,15] inhibits nitrous oxide- and isoflurane-induced neuronal death (and the consequent cognitive impairment) in newborn rats[13] and blunts the death of neurons triggered by the occlusion of the middle cerebral artery in rodents.[8] In addition, xenon reportedly reduces the lethal response to cold injury of organotypic cultures of rat hippocampus,[8,9] as well as the *N*-methyl-*D*-aspartate (NMDA)-induced influx of Ca^{2+} ions in cultured neurons,[8] an event that is critically involved in excitotoxicity.[29] Xenon has also been shown to protect isolated rabbit hearts from ischemia/reperfusion injury,[16] an effect that was abolished by the specific mitoK_{ATP} channel blocker 5-hydroxydecanoate.[16] Along similar lines, xenon limits the mid-term ventricular remodeling triggered by myocardial infarction in neonate rats, resulting in improved contractility and increased ejection fraction.[18] Finally, xenon has been shown to reduce the renal allograft injury that is generally associated with prolonged hypothermic graft storage in multiple rat models of transplantation.[4,19,20] Of note, the effects of xenon may exhibit some degree of context dependency, as some reports indicate that, at least under specific circumstances, xenon mediates cytotoxic, rather than cytoprotective, effects in vitro and in vivo.[40,41]

In contrast to the abundant literature dealing with xenon, only a few studies have previously alluded to the cytoprotective potential of argon. One such work demonstrated that argon can reduce neuronal apoptosis in fetal cortical slices exposed to oxygen and glucose deprivation in vitro.[10] In addition, argon reportedly shares with xenon the ability to improve the cytoprotective effects of hypothermic storage in a rat model of renal transplantation, significantly improving the functions of the graft.[4] In this setting, however, 2 additional, potent cytoprotective interventions were employed, hypothermia and complete oxygen depletion. Conversely, here we replaced nitrogen with inert gases, leaving the concentrations of both oxygen and carbon dioxide unaltered, and used metabolically active, proliferating cells.

The expression "noble gas" translates the German word "edelgas", a term that points to the extremely low chemical reactivity of these elements. It may therefore seem surprising that only 2 among the 5 noble gases tested here turned out to mediate cytoprotective effects. Moreover, these 2 gases, argon and xenon, are separated in Mendeleev's periodic table by another element, krypton. These observations underscore the difficulty to apprehend the mode of action of noble gases and their effects on biological systems. Notwithstanding these caveats, argon and xenon appear to share a broad antiapoptotic activity that might be harnessed for several distinct experimental and clinical applications.

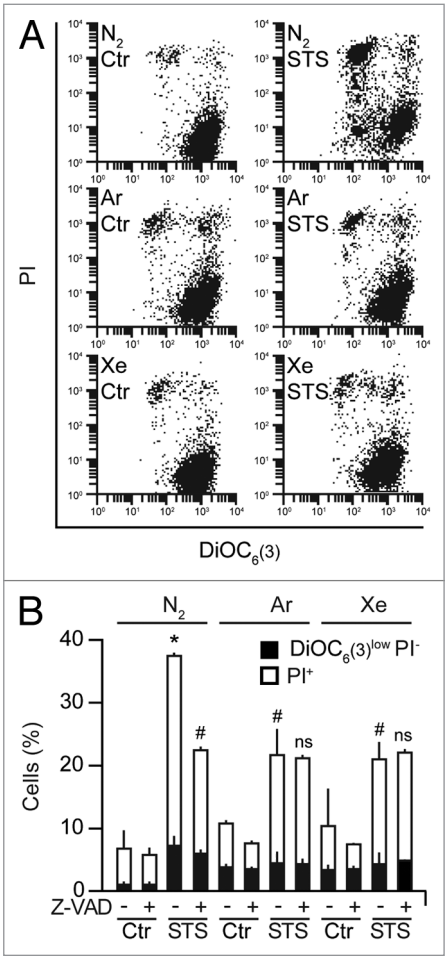

Figure 3. Antiapoptotic effects of argon and xenon. (**A and B**) Wild-type human osteosarcoma U2OS cells were left untreated or treated with 1 μM staurosporine (STS), 50 μM Z-VAD-fmk (Z-VAD), or both in control atmospheric conditions (N_2) or in the presence of gas mixtures, in which N_2 was specifically replaced with Ar or Xe, for 8 h. Thereafter, cells were processed for the cytofluorometric assessment of apoptosis-related upon $DiOC_6(3)$/propidium iodide (PI) co-staining. Representative dot plots are depicted in (**A**), while quantitative data are in (**B**). In (**B**), black and white column illustrate the percentage of dead (PI^+) or dying ($PI^-DiOC_6[3]^{low}$) cells, respectively (means ± SD). *$P < 0.05$ (Student *t* test), as compared with untreated cells maintained in control atmospheric conditions. #$P < 0.05$ (Student *t* test), as compared with cells treated with STS in control atmospheric conditions; ns, non significant (Student *t* test), as compared with cells treated with STS and Z-VAD in equal atmospheric conditions.

Material and Methods

Cell culture and treatments

Unless otherwise indicated, chemicals were purchased from Sigma-Aldrich, while media and supplement for cell culture were from Gibco®-Life Technologies™. Wild-type human osteosarcoma U2OS cells were obtained from the American Type Culture Collection (ATCC) and maintained in Dulbecco modified essential medium (DMEM) supplemented with 10% fetal bovine serum (FBS), 10 mM HEPES buffer, 100 units/mL penicillin sodium, 100 μg/mL streptomycin sulfate, and 1X non-essential amino acids. The generation of U2OS cells stably expressing H2B-RFP or green fluorescence protein (GFP)-LC3 chimeras has previously been described.[42-44] Genetically modified U2OS cells were propagated in the presence of 5 μg/mL blasticidine.

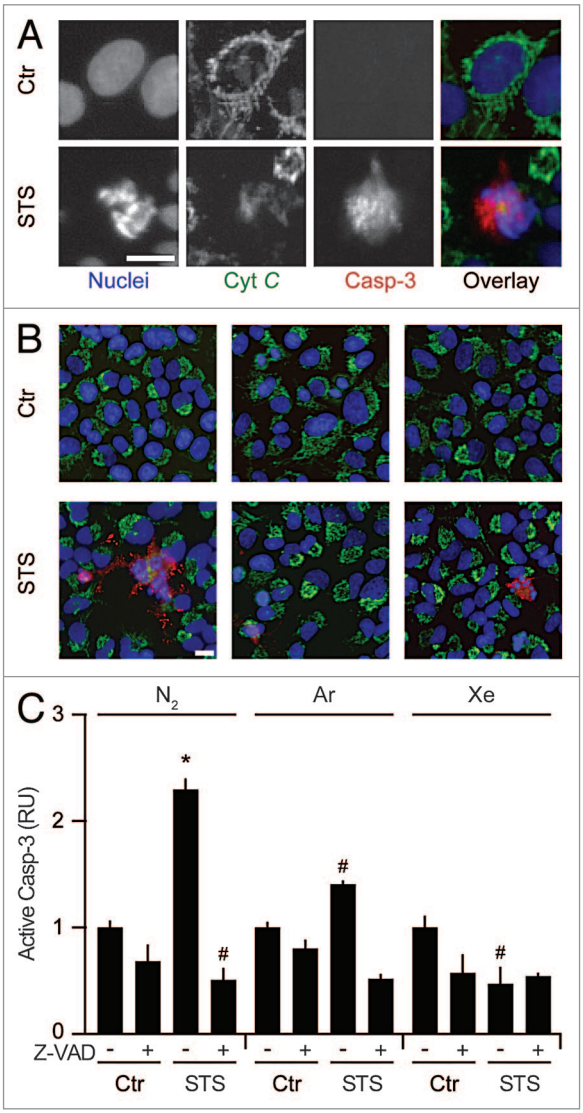

Figure 4. Argon- and xenon-mediated inhibition of mitochondrial membrane permeabilization and caspase activation. (**A–C**) Wild-type human osteosarcoma U2OS cells were left untreated or treated with 1 μM staurosporine (STS), 50 μM Z-VAD-fmk (Z-VAD) or both, in control atmospheric conditions (N_2) or in the presence of gas mixtures in which N_2 was specifically replaced with Ar or Xe for 8 h. Thereafter, cells were processed for the assessment of cytochrome *c* (Cyt *C*) release and caspase-3 (Casp-3) activation by robotized immunofluorescence microscopy coupled to automated imaging. Representative images are reported in (**A and B**) (scale bar = 10 μm), while normalized quantitative data on Casp-3 activation (RU, means ± SD, calculated on > 500 cells per conditions) are illustrated in (**C**). **P* < 0.05 (Student *t* test), as compared with untreated cells maintained in control atmospheric conditions. #*P* < 0.05 (Student *t* test), as compared with cells treated with STS in control atmospheric conditions.

Gas exposure

Five thousand H2B-RFP- or GFP-LC3-expressing cells were seeded in 96-well BD Falcon™ black/clear imaging plates (BD Biosciences) and maintained under standard culture conditions (200 μL medium/well, 37 °C, 5% CO_2) for 24 h. Thereafter, 160 μL medium were removed from each well and replaced with 150 μL of fresh medium that had previously been saturated with pre-determined gas mixtures by bubbling (flow rate = 1 L/min, 10 min). Ten μL of drug-free culture medium or medium containing a 20× concentration of the chemicals employed in this study were employed to restore a final culture volume of 200 μL, and plates were transferred into System Duetz gas-tight chambers (Enzyscreen). Upon verification of the tightness of the chamber, gas mixtures were washed in (flow rate = 10 L/min), until CO_2 concentrations at the outlet and inlet ports of the chamber, measured by a g100 gas analyzer (GeoTech), were equivalent. Chambers were incubated at 37 °C in the dark for 6 or 16 h, after which cells were fixed with 3.7% paraformaldehyde (w:v in PBS), optionally supplemented with 1 μg/mL Hoechst 33342 (Molecular Probes®-Life Technologies™) for 20 min. Eventually, the fixative was replaced with PBS, and plates were either destined to automated imaging as such (for the assessment of cell number) or further processed for immunostaining (to determine cytochrome c release and caspase-3 activation). Gases were manipulated and stored following common safety rules and institutional guidelines. Gas mixtures were kept at room temperature for at least 48 h before the experiment to avoid liquefaction-related changes in composition.

Assessment of cytochrome *c* release and caspase-3 activation

Cytochrome *c* release and caspase-3 activation were monitored by automated imaging upon immunostaining with specific antibodies, as previously described[45,46] To this aim, cells fixed and stained with Hoechst 33342 as described above were washed once in PBS and permeabilized with 0.1% Triton X100 (v:v in PBS), followed by the blocking of unspecific binding sites with 2% bovine serum albumin (w:v in PBS). Thereafter, cells were sequentially immunostained with primary antibodies, specific for cytochrome *c* (rabbit monoclonal IgG1 # 556432, BD Biosciences) and active caspase-3 (CASP3a, rabbit monoclonal IgG #9661, Cell Signaling Technology Inc), and appropriate Alexa Fluor conjugates (Molecular Probes®-Life Technologies™). Upon 2 washes in PBS, plates were subjected to automated imaging.

Automated image acquisition and analysis

For automated (immuno)fluorescence microscopy, a robot-assisted BD Pathway 855 High-Content BioImager (BD Biosciences) equipped with Photofluor light sources

(Chroma), multiple excitation and emission filters (Semrock) and an ORCA-AG Deep Cooled Digital Camera (Hamamatsu Photonics) was used to acquire at least 4 viewfields per sample (20× magnification).

Images were automatically processed by means of the BD AttoVision™ software version 1.7 (BD Biosciences). In particular, the following regions of interests (ROIs) were defined: nuclei, identified using the H2B-RFP or Hoechst 33342 signals; and cells, defined by the nuclear area plus a perinuclear extension of 10 pixels. Objects were equalized and contrasted from the background by means of shading and rolling-ball pre-processing filters, followed by automatic signal-to-noise thresholding. To exclude events corresponding to more than one nucleus from the analysis, successful segregation of each nucleus as a unique ROI was conducted using an open pre-processing filter combined with a watershed erosion algorithm. The putative bias coming from cellular debris of overlapping clusters of nuclei was eluded by applying a "scrap" algorithm set to minimal and maximal size limits of 50 and 2500 pixels, respectively.

Cytofluorometry

To monitor apoptosis-associated parameters, cells were co-stained with 1 μg/mL propidium iodide (PI) (Sigma-Aldrich), which identifies cells with ruptured plasma membranes, and 40 nM 3,3′dihexiloxalocarbocyanine iodide ($DiOC_6$[3]; Molecular Probes®-Life Technologies™), which measures $\Delta\psi_m$, as previously reported.[47,48] Cytofluorometric acquisitions were performed on a FACSCalibur™ cytometer (BD Biosciences), and first-line statistical analyses were with the CellQuest™ software (BD Biosciences) upon gating on the events characterized by normal forward and side scatter.

Statistical procedures

Unless otherwise specified, experiments were performed in triplicate instances. Data were analyzed with Excel (Microsoft Co) and Prism 5 (GraphPad Software Inc). Raw data on cell number and caspase-3 activation were obtained from a population of at least 100 cells per experimental condition, in duplicate parallel instances, and normalized to appropriate control values. Statistical significance was assessed by means of Student *t*-tests. *P* values < 0.05 were considered statistically significant.

Disclosure of Potential Conflicts of Interest

No potential conflicts of interest were disclosed.

Acknowledgments

The authors are supported by the Ligue contre le Cancer (équipe labelisée), Agence National de la Recherche, AXA Chair for Longevity Research, Association pour la Recherche sur le Cancer, Cancéropôle Ile-de-France, Institut National du Cancer (INCa), Fondation Bettencourt-Schueller, Fondation de France, Fondation pour la Recherche Médicale, the European Commission (ArtForce), the European Research Council, the LabEx Immuno-Oncology, the SIRIC Stratified Oncology Cell DNA Repair and Tumor Immune Elimination (Socrate) and Cancer Research and Personalized Medicine (Carpem) and the Paris Alliance of Cancer Research Institutes (PACRI). This study was supported by a specific grant from Air Liquide.

References

1. Hausenloy DJ, Yellon DM. The therapeutic potential of ischemic conditioning: an update. Nat Rev Cardiol 2011; 8:619-29; PMID:21691310; http://dx.doi.org/10.1038/nrcardio.2011.85
2. Gidday JM. Cerebral preconditioning and ischaemic tolerance. Nat Rev Neurosci 2006; 7:437-48; PMID:16715053; http://dx.doi.org/10.1038/nrn1927
3. Brücken A, Cizen A, Fera C, Meinhardt A, Weis J, Nolte K, et al. Argon reduces neurohistopathological damage and preserves functional recovery after cardiac arrest in rats. Br J Anaesth 2013; 110(Suppl 1):i106-12; PMID:23393152; http://dx.doi.org/10.1093/bja/aes509
4. Irani Y, Pype JL, Martin AR, Chong CF, Daniel L, Gaudart J, et al. Noble gas (argon and xenon)-saturated cold storage solutions reduce ischemia-reperfusion injury in a rat model of renal transplantation. Nephron Extra 2011; 1:272-82; PMID:22470401; http://dx.doi.org/10.1159/000335197
5. Ryang YM, Fahlenkamp AV, Rossaint R, Wesp D, Loetscher PD, Beyer C, et al. Neuroprotective effects of argon in an in vivo model of transient middle cerebral artery occlusion in rats. Crit Care Med 2011; 39:1448-53; PMID:21336110; http://dx.doi.org/10.1097/CCM.0b013e31821209be
6. Schiltz M, Fourme R, Broutin I, Prangé T. The catalytic site of serine proteinases as a specific binding cavity for xenon. Structure 1995; 3:309-16; PMID:7788296; http://dx.doi.org/10.1016/S0969-2126(01)00161-7
7. Preckel B, Weber NC, Sanders RD, Maze M, Schlack W. Molecular mechanisms transducing the anesthetic, analgesic, and organ-protective actions of xenon. Anesthesiology 2006; 105:187-97; PMID:16810011; http://dx.doi.org/10.1097/00000542-200607000-00029
8. Abraini JH, David HN, Lemaire M. Potentially neuroprotective and therapeutic properties of nitrous oxide and xenon. Ann N Y Acad Sci 2005; 1053:289-300; PMID:16179534; http://dx.doi.org/10.1196/annals.1344.025
9. Bickler PE, Warren DE, Clark JP, Gabatto P, Gregersen M, Brosnan H. Anesthetic protection of neurons injured by hypothermia and rewarming: roles of intracellular Ca2+ and excitotoxicity. Anesthesiology 2012; 117:280-92; PMID:22728782; http://dx.doi.org/10.1097/ALN.0b013e318260a7b9
10. Jawad N, Rizvi M, Gu J, Adeyi O, Tao G, Maze M, et al. Neuroprotection (and lack of neuroprotection) afforded by a series of noble gases in an in vitro model of neuronal injury. Neurosci Lett 2009; 460:232-6; PMID:19500647; http://dx.doi.org/10.1016/j.neulet.2009.05.069
11. Luo Y, Ma D, Ieong E, Sanders RD, Yu B, Hossain M, et al. Xenon and sevoflurane protect against brain injury in a neonatal asphyxia model. Anesthesiology 2008; 109:782-9; PMID:18946288; http://dx.doi.org/10.1097/ALN.0b013e3181895f88
12. Ma D, Hossain M, Pettet GK, Luo Y, Lim T, Akimov S, et al. Xenon preconditioning reduces brain damage from neonatal asphyxia in rats. J Cereb Blood Flow Metab 2006; 26:199-208; PMID:16034370; http://dx.doi.org/10.1038/sj.jcbfm.9600184
13. Shu Y, Patel SM, Pac-Soo C, Fidalgo AR, Wan Y, Maze M, et al. Xenon pretreatment attenuates anesthetic-induced apoptosis in the developing brain in comparison with nitrous oxide and hypoxia. Anesthesiology 2010; 113:360-8; PMID:20613483; http://dx.doi.org/10.1097/ALN.0b013e3181d960d7
14. Faulkner S, Bainbridge A, Kato T, Chandrasekaran M, Kapetanakis AB, Hristova M, et al. Xenon augmented hypothermia reduces early lactate/N-acetylaspartate and cell death in perinatal asphyxia. Ann Neurol 2011; 70:133-50; PMID:21674582; http://dx.doi.org/10.1002/ana.22387
15. Yang T, Zhuang L, Rei Fidalgo AM, Petrides E, Terrando N, Wu X, et al. Xenon and sevoflurane provide analgesia during labor and fetal brain protection in a perinatal rat model of hypoxia-ischemia. PLoS One 2012; 7:e37020; PMID:22615878; http://dx.doi.org/10.1371/journal.pone.0037020
16. Li Q, Lian C, Zhou R, Li T, Xiang X, Liu B. Pretreatment with xenon protected immature rabbit heart from ischaemia/reperfusion injury by opening of the mitoKATP channel. Heart Lung Circ 2013; 22:276-83; PMID:23261327; http://dx.doi.org/10.1016/j.hlc.2012.10.016
17. Hein M, Roehl AB, Baumert JH, Bantes B, Bleilevens C, Bernstein N, et al. Establishment of a porcine right ventricular infarction model for cardioprotective actions of xenon and isoflurane. Acta Anaesthesiol Scand 2008; 52:1194-203; PMID:18823457; http://dx.doi.org/10.1111/j.1399-6576.2008.01757.x
18. Roehl AB, Funcke S, Becker MM, Goetzenich A, Bleilevens C, Rossaint R, et al. Xenon and isoflurane reduce left ventricular remodeling after myocardial infarction in the rat. Anesthesiology 2013; 118:1385-94; PMID:23364599; http://dx.doi.org/10.1097/ALN.0b013e31828744c0
19. Zhao H, Yoshida A, Xiao W, Ologunde R, O'Dea KP, Takata M, et al. Xenon treatment attenuates early renal allograft injury associated with prolonged hypothermic storage in rats. FASEB J 2013; PMID:23759444; http://dx.doi.org/10.1096/fj.13-232173
20. Zhao H, Watts HR, Chong M, Huang H, Tralau-Stewart C, Maxwell PH, et al. Xenon Treatment Protects Against Cold Ischemia Associated Delayed Graft Function and Prolongs Graft Survival in Rats. Am J Transplant 2013; PMID:23710625; http://dx.doi.org/10.1111/ajt.12293

21. Bantel C, Maze M, Trapp S. Noble gas xenon is a novel adenosine triphosphate-sensitive potassium channel opener. Anesthesiology 2010; 112:623-30; PMID:20179498; http://dx.doi.org/10.1097/ALN.0b013e3181cf894a
22. Garlid KD, Halestrap AP. The mitochondrial K(ATP) channel--fact or fiction? J Mol Cell Cardiol 2012; 52:578-83; PMID:22240339; http://dx.doi.org/10.1016/j.yjmcc.2011.12.011
23. Galluzzi L, Maiuri MC, Vitale I, Zischka H, Castedo M, Zitvogel L, et al. Cell death modalities: classification and pathophysiological implications. Cell Death Differ 2007; 14:1237-43; PMID:17431418; http://dx.doi.org/10.1038/sj.cdd.4402148
24. Kroemer G, Galluzzi L, Vandenabeele P, Abrams J, Alnemri ES, Baehrecke EH, et al.; Nomenclature Committee on Cell Death 2009. Classification of cell death: recommendations of the Nomenclature Committee on Cell Death 2009. Cell Death Differ 2009; 16:3-11; PMID:18846107; http://dx.doi.org/10.1038/cdd.2008.150
25. Kroemer G, Galluzzi L, Brenner C. Mitochondrial membrane permeabilization in cell death. Physiol Rev 2007; 87:99-163; PMID:17237344; http://dx.doi.org/10.1152/physrev.00013.2006
26. Galluzzi L, Vitale I, Abrams JM, Alnemri ES, Baehrecke EH, Blagosklonny MV, et al. Molecular definitions of cell death subroutines: recommendations of the Nomenclature Committee on Cell Death 2012. Cell Death Differ 2012; 19:107-20; PMID:21760595; http://dx.doi.org/10.1038/cdd.2011.96
27. Vitale I, Galluzzi L, Castedo M, Kroemer G. Mitotic catastrophe: a mechanism for avoiding genomic instability. Nat Rev Mol Cell Biol 2011; 12:385-92; PMID:21527953; http://dx.doi.org/10.1038/nrm3115
28. Galluzzi L, Joza N, Tasdemir E, Maiuri MC, Hengartner M, Abrams JM, et al. No death without life: vital functions of apoptotic effectors. Cell Death Differ 2008; 15:1113-23; PMID:18309324; http://dx.doi.org/10.1038/cdd.2008.28
29. Galluzzi L, Blomgren K, Kroemer G. Mitochondrial membrane permeabilization in neuronal injury. Nat Rev Neurosci 2009; 10:481-94; PMID:19543220; http://dx.doi.org/10.1038/nrn2665
30. Feng G, Kaplowitz N. Mechanism of staurosporine-induced apoptosis in murine hepatocytes. Am J Physiol Gastrointest Liver Physiol 2002; 282:G825-34; PMID:11960779
31. Kepp O, Tesniere A, Zitvogel L, Kroemer G. The immunogenicity of tumor cell death. Curr Opin Oncol 2009; 21:71-6; PMID:19125021; http://dx.doi.org/10.1097/CCO.0b013e32831bc375
32. Lindahl PE, Oberg KE. Mechanism of the physiological action of rotenone. Nature 1960; 187:784; PMID:14417054; http://dx.doi.org/10.1038/187784a0
33. Slater EC. The mechanism of action of the respiratory inhibitor, antimycin. Biochim Biophys Acta 1973; 301:129-54; PMID:4358868; http://dx.doi.org/10.1016/0304-4173(73)90002-5
34. Marchetti P, Susin SA, Decaudin D, Gamen S, Castedo M, Hirsch T, et al. Apoptosis-associated derangement of mitochondrial function in cells lacking mitochondrial DNA. Cancer Res 1996; 56:2033-8; PMID:8616847
35. Galluzzi L, Aaronson SA, Abrams J, Alnemri ES, Andrews DW, Baehrecke EH, et al. Guidelines for the use and interpretation of assays for monitoring cell death in higher eukaryotes. Cell Death Differ 2009; 16:1093-107; PMID:19373242; http://dx.doi.org/10.1038/cdd.2009.44
36. Kepp O, Galluzzi L, Lipinski M, Yuan J, Kroemer G. Cell death assays for drug discovery. Nat Rev Drug Discov 2011; 10:221-37; PMID:21358741; http://dx.doi.org/10.1038/nrd3373
37. Michaud M, Martins I, Sukkurwala AQ, Adjemian S, Ma Y, Pellegatti P, et al. Autophagy-dependent anticancer immune responses induced by chemotherapeutic agents in mice. Science 2011; 334:1573-7; PMID:22174255; http://dx.doi.org/10.1126/science.1208347
38. Shen S, Niso-Santano M, Adjemian S, Takehara T, Malik SA, Minoux H, et al. Cytoplasmic STAT3 represses autophagy by inhibiting PKR activity. Mol Cell 2012; 48:667-80; PMID:23084476; http://dx.doi.org/10.1016/j.molcel.2012.09.013
39. Vitale I, Senovilla L, Jemaà M, Michaud M, Galluzzi L, Kepp O, et al. Multipolar mitosis of tetraploid cells: inhibition by p53 and dependency on Mos. EMBO J 2010; 29:1272-84; PMID:20186124; http://dx.doi.org/10.1038/emboj.2010.11
40. Cattano D, Williamson P, Fukui K, Avidan M, Evers AS, Olney JW, et al. Potential of xenon to induce or to protect against neuroapoptosis in the developing mouse brain. Can J Anaesth 2008; 55:429-36; PMID:18591700; http://dx.doi.org/10.1007/BF03016309
41. Brosnan H, Bickler PE. Xenon Neurotoxicity in Rat Hippocampal Slice Cultures Is Similar to Isoflurane and Sevoflurane. Anesthesiology 2013; PMID:23591069; http://dx.doi.org/10.1097/ALN.0b013e31829417f0
42. Criollo A, Senovilla L, Authier H, Maiuri MC, Morselli E, Vitale I, et al. IKK connects autophagy to major stress pathways. Autophagy 2010; 6:189-91; PMID:20110771; http://dx.doi.org/10.4161/auto.6.1.10818
43. Martins I, Kepp O, Schlemmer F, Adjemian S, Tailler M, Shen S, et al. Restoration of the immunogenicity of cisplatin-induced cancer cell death by endoplasmic reticulum stress. Oncogene 2011; 30:1147-58; PMID:21151176; http://dx.doi.org/10.1038/onc.2010.500
44. Rello-Varona S, Kepp O, Vitale I, Michaud M, Senovilla L, Jemaà M, et al. An automated fluorescence videomicroscopy assay for the detection of mitotic catastrophe. Cell Death Dis 2010; 1:e25; PMID:21364633; http://dx.doi.org/10.1038/cddis.2010.6
45. de La Motte Rouge T, Galluzzi L, Olaussen KA, Zermati Y, Tasdemir E, Robert T, et al. A novel epidermal growth factor receptor inhibitor promotes apoptosis in non-small cell lung cancer cells resistant to erlotinib. Cancer Res 2007; 67:6253-62; PMID:17616683; http://dx.doi.org/10.1158/0008-5472.CAN-07-0538
46. Hoffmann J, Vitale I, Buchmann B, Galluzzi L, Schwede W, Senovilla L, et al. Improved cellular pharmacokinetics and pharmacodynamics underlie the wide anticancer activity of sagopilone. Cancer Res 2008; 68:5301-8; PMID:18593931; http://dx.doi.org/10.1158/0008-5472.CAN-08-0237
47. Galluzzi L, Morselli E, Vitale I, Kepp O, Senovilla L, Criollo A, et al. miR-181a and miR-630 regulate cisplatin-induced cancer cell death. Cancer Res 2010; 70:1793-803; PMID:20145152; http://dx.doi.org/10.1158/0008-5472.CAN-09-3112
48. Galluzzi L, Vitale I, Senovilla L, Olaussen KA, Pinna G, Eisenberg T, et al. Prognostic impact of vitamin B6 metabolism in lung cancer. Cell Rep 2012; 2:257-69; PMID:22854025; http://dx.doi.org/10.1016/j.celrep.2012.06.017